Electronic Supplementary Information for

Physical adsorption of OH^- causes anomalous charging at oxide-water interface

Yingchun Zhang,[a] Yong-Bin Zhuang,[b] Xiandong Liu,*[a] Jun Cheng,*[b,c] Johannes Lützenkirchen*[d] and Xiancai Lu[a]

[a]State Key Laboratory for Mineral Deposits Research, School of Earth Sciences and Engineering, Nanjing University, Nanjing, Jiangsu 210023, P. R. China

[b]State Key Laboratory of Physical Chemistry of Solid Surfaces, iChEM, College of Chemistry and Chemical Engineering, Xiamen University, Xiamen, Fujian 361005, P. R. China

[c]Tan Kah Kee Innovation Laboratory, Xiamen University, Xiamen, Fujian 361005, P. R. China

[d]Institute of Nuclear Waste Disposal (INE), Karlsruhe Institute of Technology (KIT), 76344 Eggenstein-Leopoldshafen, Germany

*Corresponding author. Email: xiandongliu@nju.edu.cn, chengjun@xmu.edu.cn, johannes.luetzenkirchen@kit.edu

Number of pages: 12

Number of tables: 3

Number of figures: 5

This document includes the following contents:

S1 Methodology

S1.1 Models

The crystal structure data reported in Ref. 1 were used to build the surface model: a=b=4.757 Å, c=12.9877 Å and α=β=90°, γ=120°. The (0001) surface model (Fig. S1) consisted of 2×2×1 unit cells and was cut from the bulk crystal based on the structure derived by CTR and X-ray reflectivity (XR) studies,[2,3] where the O atoms on the surfaces were all protonated and every OH group bridged two subsurface Al atoms (i.e. Al_2OH).

The surface model was placed in a 3D periodically repeated cell of 9.514×9.514×30.000 $Å^3$. The cell had a solution region of ~16 Å in the direction perpendicular to the surface. 42 water molecules were placed in the solution region, which approximately reproduces the density of bulk water under ambient conditions. For the OH^- containing system, one OH^- was inserted into the solution at an initial position of 5.5 Å from the plane of surface O atoms.

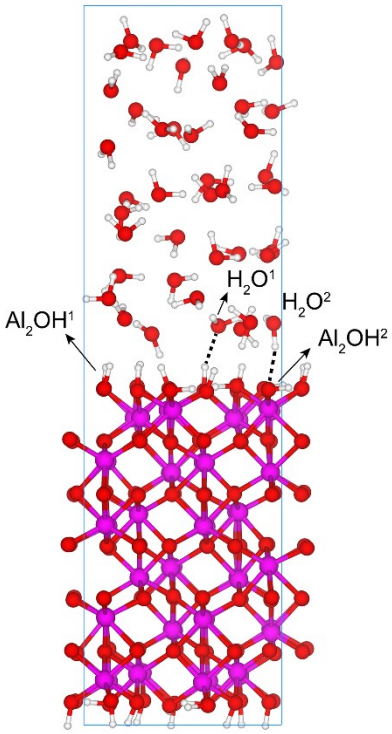

Fig. S1. The corundum (0001) surface model used in the present study. Al_2OH^1 and Al_2OH^2 mark the two differently oriented surface groups. Two kinds of water molecules that hydrogen bonded with surface groups (i.e. H_2O^1 and H_2O^2) are also indicated. O = red, H = white, Al = purple.

Adsorption of OH^- on another two OH covered surface, i.e., gibbsite (001)-water and Ga_2O_3 (0001)-water interfaces was also investigated. These two surfaces have similar surface structures to corundum (0001) surface. The crystal structure parameters used for building the gibbsite (001) surface model were a = 8.742 Å, b = 5.112 Å, c = 9.801 Å and $\alpha = \gamma = 90°$, $\beta = 94.54°$.[4] The cell parameters used for building Ga_2O_3 (0001) surface were $a = b$ = 4.997 Å, c = 13.451 Å and $\alpha = \beta = 90°$, $\gamma = 120°$. The gibbsite (001) surface model contained 1 × 2 × 1 unit cells and the Ga_2O_3 (0001) surface model contained 2 × 2 × 1 unit cells. Both surface models were surmounted by a ~16 Å thick solution region that contained 48 and 46 water molecules for gibbsite (001) and Ga_2O_3 (0001) surface models respectively. The simulation box had the dimensions of 8.742 × 10.224 × 25.770 $Å^3$ for gibbsite (001) surface (Fig. S2A) and 9.995 × 9.995 × 31.0 $Å^3$ for Ga_2O_3 (0001) surface (Fig. S2B).

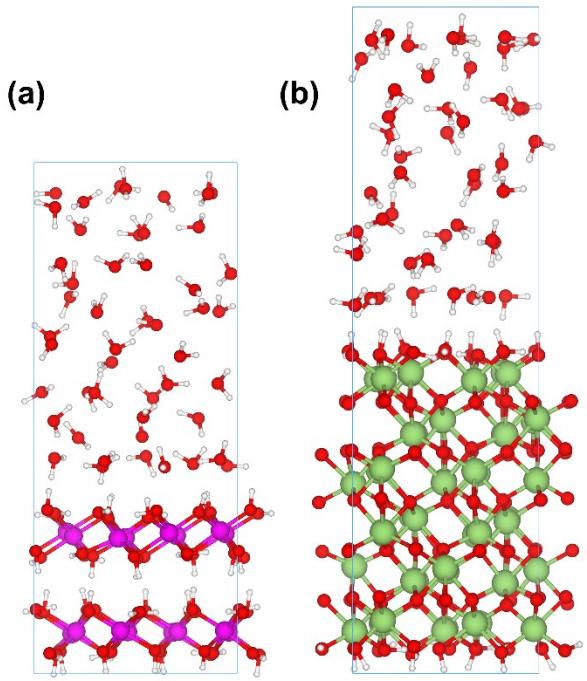

Fig. S2. The gibbsite (001) surface model (A) and Ga_2O_3 (0001) surface model (B) used in the present study. O = red, H = white, Al = purple, Ga = green.

S1.2 *ab initio* molecular dynamics (AIMD)

The CP2K/QUICKSTEP package[5,6] was applied to carry out the AIMD simulations. With this code, the electronic structures were calculated with density functional theory implemented with a hybrid Gaussian plane wave (GPW) approach[7]. PBE functional[8] and Goedecker-Teter-Hutter pseudopotentials[9] were used. van der Waals corrections were included with the DFT-D3 method.[10] The plane wave basis cutoff for the electron density was set to 360 Ry. For the charged systems, the net charges were neutralized by adding a background charge as implemented in the CP2K/QUICKSTEP code.

Born-Oppenheimer type molecular dynamics simulations were carried out with a wave function optimization tolerance of 1.0×10^{-6}.[11] The MD timestep was 0.5 fs. The temperature was controlled at 330K by using the Nose-Hoover chain thermostat. This higher temperature was to avoid the glassy behavior of liquid water at lower temperature.[12] A free AIMD simulation was performed for ~45 ps to probe the reorientational dynamics of interfacial water. The reorientation time of bulk water was calculated from a ~60 ps AIMD trajectory of system consisted of 64 water molecules. The simulation times were enough to investigate the reorientation dynamics of water.[13,14] Three OH^--bearing systems with different initial configurations were adopted to derive the position and dynamics of OH^-. The AIMD simulations last ~35 ps, ~50 ps, and ~120 ps for the three OH^--bearing systems respectively. For the pKa calculation, a production run was performed for over 10 ps following an equilibration run of at least 5 ps.

S1.3 Calculation of pKa values

The pKa calculation technique we applied was the half-reaction scheme of the vertical energy gap method.[15,16] With this scheme, the acidic proton was transformed into a dummy atom. A proton of a hydronium located in the solution region was transformed into a dummy in the same way. The free energy changes of these processes were obtained by using the thermodynamic integration relation. The pKa value was finally derived from these free energy changes. For details, we refer to previous publications.[17-19]

In the simulations, a restrained harmonic potential (V_r) was applied to keep the dummy in a location resembling that of the acid proton in the reactant state,

$$V_r = \sum_{bonds} \frac{1}{2} k_d \left(d - d_0\right)^2 + \sum_{angles} \frac{1}{2} k_\theta \left(\theta - \theta_0\right)^2 \quad \text{* MERGEFORMAT (1)}$$

The equilibrium values used for each surface group were derived from the simulations without restraints and the force constants k_d and k_θ were selected according to previous studies.[15,16] Table S1 summarizes the parameters used in the simulations.

S1.4 Calculation of Reorientation time

The reorientation time of water molecules was extracted from AIMD trajectory by calculating the orientational time correlation function:

$$C_2(t) = \left\langle P_2[\mathbf{u}(0) \cdot \mathbf{u}(t)] \right\rangle \quad \text{* MERGEFORMAT (2)}$$

where P_2 is the second-order Legendre polynomial and $\boldsymbol{u}$ is the unit vector of a water O-H bond.[20] The reorientation time τ_2 was determined by fitting $C_2(t)$ to the function $B\exp(-t/\tau_2)$ (Fig. S3).

S2 Results

S2.1 pKas

Table S2 lists the averaged vertical energy gaps, free energy changes, and pKa values for Al_2OH^1 and Al_2OH^2H on corundum (0001) surface and two differently oriented water molecules in the first-layer water.

Table S1. The parameters used in restraining the dummy atoms (harmonic potentials in Eq. (1)). H_d represents the dummy atom. n_d and n_θ denote the number of restrained bonds and angles, respectively. d_0 stands for equilibrium bond lengths (in Bohr), and θ_0 stands for equilibrium angles (in radian).

Surface group	n_d	d_0	k_d	n_θ	θ_0	k_θ
$\equiv Al_2OH_2H_d$	1	1.91	0.1	3	1.87 (H-O-H_d)	0.1
					2.00 (Al-O-H_d)	0.1
					2.00 (Al-O-H_d)	0.1
$\equiv Al_2OH^1d$	1	1.91	0.1	2	2.00 (Al-O-H_d)	0.1
					2.00 (Al-O-H_d)	0.1
$HOH^1{}_d$	2	1.89	1.0	1	1.87 (H-O-H_d)	0.1
		1.89	1.0			
$HOH^2{}_d$	2	1.89	1.0	1	1.87 (H-O-H_d)	0.1
		1.89	1.0			
$H_2H_dO^+$	3	1.89	1.0	2	1.94 (H-O-H_d)	0.1

	1.89	1.0	1.94 (H-O-H_d)	0.1
	1.89	1.0		

Table S2. The computed vertical energy gaps (in eV), thermodynamic integrals (in eV), and pKas.

Surface group	η=1.0	η=0.75	η=0.5	η=0.25	η=0.0	ΔA	pKa
Al_2OH^1	14.68±0.01	20.13±0.02	21.33±0.01	22.43±0.01	23.20±0.01	20.90±0.01	18.0±0.4
Al_2OH^2H	16.14±0.05	19.01±0.02	19.93±0.03	21.32±0.02	22.05±0.02	19.95±0.02	1.9±0.5
H_2O^1	16.29±0.05	19.35±0.04	21.07±0.04	22.29±0.04	23.51±0.01	20.71±0.04	14.5±1.3
H_2O^2	16.06±0.01	19.37±0.01	20.92±0.01	22.28±0.05	23.43±0.04	20.66±0.03	13.7±1.2
H_3O^+	15.36±0.01	18.41±0.04	19.74±0.04	21.23±0.04	22.47±0.01	19.65±0.04	□

S2.2 Reorientation time

The calculated reorientation times for water in different layers and for bulk water were collected in Table S3. The time correlation functions and fitting curves for the first layer water and bulk water were shown in Fig. S3 as examples. It can be seen that the fitting functions can describe the correlation data very well. The reorientation time obtained for bulk water was slightly higher than the experimental results (i.e. 1.95~3.0 ps from NMR and fsIR measurements),[21-23] which is characteristic for DFT simulations. Nevertheless, the reorientation time obtained for bulk water was almost identical (i.e. 5.5 V.S. 5.7) to the value reported in Ref. [14] using the same settings, which validates our calculations. The reorientation time of interfacial water decreased as the distance from corundum (0001) surface increased. The reorientation of the first-layer water was three times slower than the bulk water while the third-layer water was already bulk-like.

Table S3. The calculated reorientation time for water.

Location of water	Reorientation time (ps)
1st layer	18.6
2nd layer	7.8
3rd layer	6.6
bulk	5.5

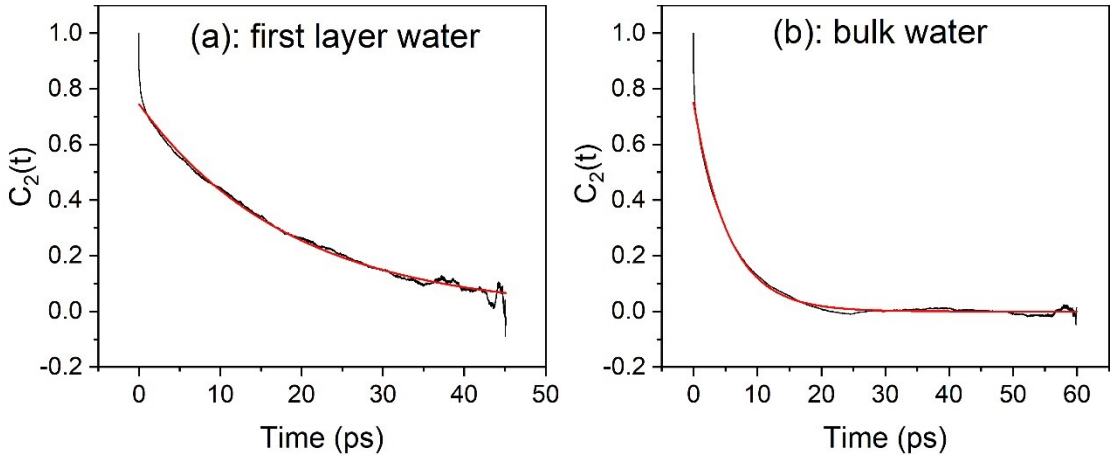

Fig. S3. The orientational time correlation functions and fitting curves. (A) the first layer water and **(B)** bulk water.

S2.3 Additional trajectories for OH^- adsorption on corundum (0001)-water interface

Adsorption of OH^- observed in the present study is independent of its initial positions. To support this conclusion, two additional AIMD simulations on corundum (0001)-water interface were performed. The evolution of the height of OH^- ion is shown in Fig. S4.

In the first trajectory (Fig. S4A), the OH^- ion was initially placed 6.5 Å from the surface. At ~6.8 ps, the OH^- ion transferred to the first water layer after three successive successful jumps. OH^- adjusted its positions during 6.8~19.8 ps and kept above the corundum (0001) surface for the following ~14.0 ps. OH^- jumped into the second water layer temporarily (~2.0 ps) and returned above the mineral surface in the rest of the trajectory.

In the second trajectory (Fig. S4B), the OH^- ion was initially placed 8.5 Å from the surface. The OH^- ion transferred to the second water layer within 1.0 ps and stayed there for ~14.0 ps. It went up to the third water layer temporarily and jumped to the top of the first water layer at ~19.7 ps. OH^- kept at this position for the following ~44.0 ps with occasional jumps to the mineral surface. At ~63.7 ps, OH^- transferred above the mineral surface and stayed for the following 48.0 ps. It then left the first water layer temporarily for ~5.0 ps and jumped back above the mineral surface.

Based on these trajectories, it can be found that OH^- ion shows staged diffusion in all of these trajectories and its dynamics is independent of the initial conditions. These different trajectories also indicate that the first water layer can indeed trap the OH^- ion effectively.

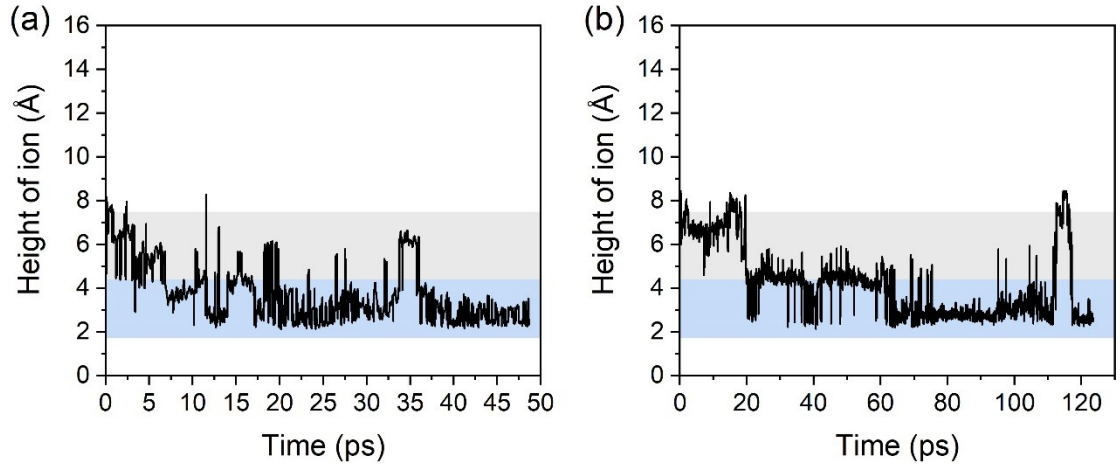

Fig. S4. Height of OH^- ion as a function of simulation time. The plane of the outermost surface O is taken as the origin of the y-axis. Initial positions of OH^- ion were **(A)** 6.5 Å and **(B)** 8.5 Å from the surface.

S2.4 OH^- adsorption on gibbsite (001)-water and Ga_2O_3 (0001)-water interfaces

On gibbsite (001)-water interface, the OH^- ion was initially placed ~6.5 Å from the surface (Fig. S5A). The OH^- ion stayed in the second layer for ~8.6 ps before it moved into the third water layer. At ~18.7 ps, the OH^- ion transferred from the third layer to the second water layer where it stayed for less than 3 ps and diffused into the first water layer. OH^- ion kept in the first layer for the following 43 ps and both parallel and vertical orientations were observed for OH^- in the first water layer.

On Ga_2O_3 (0001)-water interface, the OH^- ion was initially placed 6.7 Å from the surface (Fig. S5B). After two successful proton transfers, the OH^- ion jumped into the first water layer within less than 1 ps. It stayed on the interface for about 3 ps with occasional jumps to the bottom of the second layer. At ~4.0 ps, the OH^- moved to the bottom of the second layer and stayed there for 4.3 ps. Then the OH^- ion jumped back onto the surface and stayed in the first layer for the following ~20 ps, during which there were several unsuccessful proton transfer attempts as indicated by the spikes on the curve. On Ga_2O_3 (0001)-water interface, the hydrogen bonding environment of OH^- was similar to that on corundum (0001) and both parallel and vertical orientations were observed.

Based on these trajectories, it can be stated that apart from corundum-water interface, OH^- ion can also be trapped on gibbsite-water and Ga_2O_3-water interfaces. These observations indicate that the proposed charging mechanism indeed applies for other OH covered surfaces.

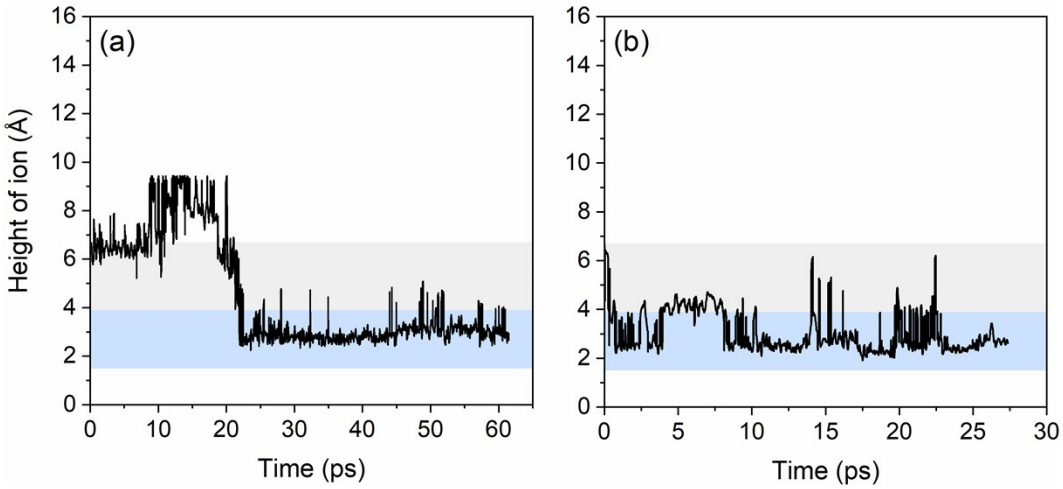

Fig. S5. Heights of OH^- ion on (A) gibbsite (001)-water and (B) Ga_2O_3 (0001)-water interfaces as a function of simulation time. The plane of the outermost surface O is taken as the origin of the y-axis.

References

1 A. Kirfel and K. Eichhorn, Accurate structure analysis with synchrotron radiation. The electron density in Al2O3 and Cu2O, *Acta Crystallogr. Sect. A*, 1990, **46**, 271-284.

2 P. J. Eng, T. P. Trainor, G. E. Brown Jr, G. A. Waychunas, M. Newville, S. R. Sutton and M. L. Rivers, Structure of the Hydrated α-Al2O3 (0001) Surface, *Science*, 2000, **288**, 1029.

3 J. G. Catalano, Weak interfacial water ordering on isostructural hematite and corundum (001) surfaces, *Geochim. Cosmochim. Acta*, 2011, **75**, 2062-2071.

4 E. Balan, M. Lazzeri, G. Morin and F. Mauri, First-principles study of the OH-stretching modes of gibbsite, *Am. Mineral.*, 2006, **91**, 115-119.

5 J. VandeVondele, M. Krack, F. Mohamed, M. Parrinello, T. Chassaing and J. Hutter, Quickstep: Fast and accurate density functional calculations using a mixed Gaussian and plane waves approach, *Comput. Phys. Commun.*, 2005, **167**, 103-128.

6 J. Hutter, M. Iannuzzi, F. Schiffmann and J. VandeVondele, CP2K: atomistic simulations of condensed matter systems, *Wiley Interdiscip. Rev.-Comput. Mol. Sci.*, 2014, **4**, 15-25.

7 B. G. Lippert, J. Hutter and M. Parrinello, A hybrid Gaussian and plane wave density functional scheme, *Mol. Phys.*, 1997, **92**, 477-487.

8 J. P. Perdew, K. Burke and M. Ernzerhof, Generalized Gradient Approximation Made Simple, *Phys. Rev. Lett.*, 1997, **78**, 1396.

9 S. Goedecker, M. Teter and J. Hutter, Separable dual-space Gaussian pseudopotentials, *Phys. Rev. B*, 1996, **54**, 1703-1710.

10 S. Grimme, J. Antony, S. Ehrlich and H. Krieg, A consistent and accurate ab initio parametrization of density functional dispersion correction (DFT-D) for the 94 elements H-Pu, *J. Chem. Phys.*, 2010, **132**, 154104.

11 J. VandeVondele and J. Hutter, An efficient orbital transformation method for electronic structure calculations, *J. Chem. Phys.*, 2003, **118**, 4365-4369.

12 J. VandeVondele, F. Mohamed, M. Krack, J. Hutter, M. Sprik and M. Parrinello, The influence of temperature and density functional models in ab initio molecular dynamics simulation of liquid water, *J. Chem. Phys.*, 2005, **122**, 014515.

13 I. C. Lin, A. P. Seitsonen, I. Tavernelli and U. Rothlisberger, Structure and Dynamics of Liquid Water from ab Initio Molecular Dynamics—Comparison of BLYP, PBE, and revPBE Density Functionals with and without van der Waals Corrections, *J. Chem. Theory Comput.*, 2012, **8**, 3902-3910.

14 R. Réocreux, T. Jiang, M. Iannuzzi, C. Michel and P. Sautet, Structuration and Dynamics of Interfacial Liquid Water at Hydrated γ-Alumina Determined by ab Initio Molecular Simulations: Implications for Nanoparticle Stability, *ACS Appl. Nano Mater.*, 2018, **1**, 191-199.

15 M. Sulpizi and M. Sprik, Acidity constants from vertical energy gaps: density functional theory based molecular dynamics implementation, *Phys. Chem. Chem. Phys.*, 2008, **10**, 5238-5249.

16 J. Cheng, M. Sulpizi and M. Sprik, Redox potentials and pK(a) for benzoquinone from density functional theory based molecular dynamics, *J. Chem. Phys.*, 2009, **131**, 154504.

17 F. Costanzo, M. Sulpizi, R. G. D. Valle and M. Sprik, The oxidation of tyrosine and tryptophan studied by a molecular dynamics normal hydrogen electrode, *J. Chem. Phys.*, 2011, **134**, 244508.

18 J. Cheng and M. Sprik, Alignment of electronic energy levels at electrochemical interfaces, *Phys. Chem. Chem. Phys.*, 2012, **14**, 11245-11267.

19 X. Liu, J. Cheng, M. Sprik, X. Lu and R. Wang, Understanding surface acidity of gibbsite with first principles molecular dynamics simulations, *Geochim. Cosmochim. Acta*, 2013, **120**, 487-495.
20 D. Laage and J. T. Hynes, Reorientional dynamics of water molecules in anionic hydration shells, *Proc. Natl. Acad. Sci. U. S. A.*, 2007, **104**, 11167-11172.
21 R. Ludwig, NMR relaxation studies in water-alcohol mixtures: the water-rich region, *Chem. Phys.*, 1995, **195**, 329-337.
22 C. J. Fecko, J. J. Loparo, S. T. Roberts and A. Tokmakoff, Local hydrogen bonding dynamics and collective reorganization in water: Ultrafast infrared spectroscopy of HOD/D2O, *J. Chem. Phys.*, 2005, **122**, 054506.
23 Y. L. A. Rezus and H. J. Bakker, On the orientational relaxation of HDO in liquid water, *J. Chem. Phys.*, 2005, **123**, 114502.